50th AIAA Aerospace Sciences Meeting including the New Horizons Forum and Aerospace Exposition
09 - 12 January 2012, Nashville, Tennessee
AIAA 2012-0198

Modification of Boron Nitride Ceramic to Replicate Hall Effect Thruster Surface Wear

Alexander J. Satonik[1] and Joshua L. Rovey[2]
Missouri University of Science and Technology, Rolla, MO, 65409

Pristine and worn Hall-effect thruster boron nitride channel materials show significant differences in surface features, and chemical compositions. Worn thruster channels are typically created by running test thrusters in vacuum chambers for hundreds of hours. This paper studies ways to manually modified pristine samples of boron nitride without the use of a Hall-effect thruster. Sandpaper and abrasive blaster tests were used to modify surface roughness values of sample from 10,000 Å to 150,000 Å. These values match the range of surface roughness seen in worn Hall-effect thrusters. Vacuum heat treatments were preformed on samples, these treatments showed the ability to modify chemical compositions of boron nitride samples, but not in a manner matching changes seen in worn thruster channels.

Nomenclature

n	=	total number of height measurements taken
R_a	=	roughness, Å
y_i	=	height of surface irregularity at location i, Å

I. Introduction

HALL-EFFECT thrusters (HETs) are an electric spacecraft propulsion system in which thrust generation is due to acceleration of ionized propellant called plasma. Typically, an HET has an annular geometry in which an axial electric field is crossed with a radial magnetic field. A cathode emits electrons that drift in the $\vec{E} \times \vec{B}$ direction, forming an azimuthal Hall current. Neutral propellant atoms, typically xenon, are injected through the anode into an annular insulating channel. Collisions between neutral xenon atoms and electrons drifting in the Hall current produce xenon ions that are accelerated by the electric field, resulting in thrust generation. A schematic of an HET is shown in Figure 1.

Many current HET efforts are focused on developing and benchmarking models that integrate the important role of surface properties of the annular channel that contains the plasma discharge.[1-9] Wall-effects play an important role in both the lifetime and overall performance of the thruster. Properties of the channel wall can affect secondary electron emission (SEE), anomalous electron transport, and near-wall conductivity, thereby altering HET performance.[10-13] Further, wall properties are an important factor in the sputter erosion processes that are known to limit thruster lifetime.[14-17] Current HET models do not integrate a realistic wall microstructure, but instead rely on sputter yield or SEE coefficients derived from idealized material tests.[5,9,18] Our results presented below show that through various

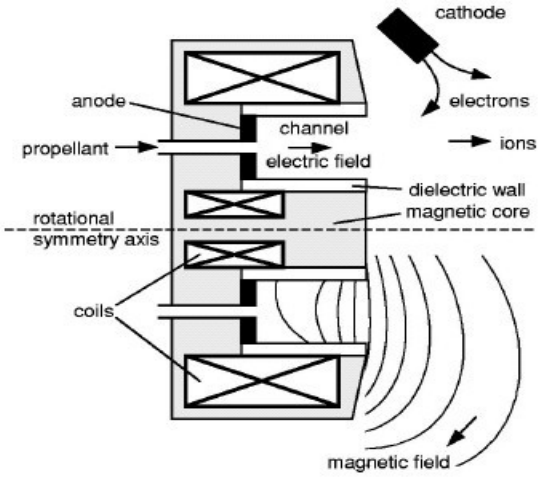

Figure 1. Schematic of a Hall Effect Thruster

[1]Graduate Research Assistant, Aerospace Plasma Lab, Mechanical & Aerospace Engineering, 160 Toomey Hall, Student Member AIAA.
[2]Assistant Professor of Aerospace Engineering, 292D Toomey Hall, Senior Member AIAA.

methods of modification some of the surface properties observed in worn HET discharge channels can be reproduced.

Properties of the HET channel wall affect SEE, anomalous electron transport, and near-wall conductivity, and erosion rate, thereby altering HET performance.[10,11] The roughness of HET channel walls has been shown to affect the equipotential contours of the plasma sheath near the channel wall reducing overall thruster performance.[19] Raitses, *et al.,* show that wall materials having higher SEE reduce the electron temperature within the HET discharge channel, thereby reducing thruster performance.[13,20] Determining the influence of material surface properties on SEE in HETs is difficult due to the complexity of electron-wall interaction, which must include factors such as roughness, composition, non-Maxwellian electron distribution, and multiple electron scattering processes all of which influence SEE yield, and as such have some level of influence on HET performance.[6] The sputter yield (atoms removed per incident ion) of the ceramic surface of a typical HET channel wall has been found to be dependent upon the roughness of the ceramic surface.[24,25]

The surface properties of the HET discharge channel change due to thruster operation. Previous results have shown that the BN channel surface changes considerably after a few 100 hours of operation. Zidar and Rovey compared pristine and worn grade HP and M26 boron nitride channel material from various locations within thrusters and showed that surface changes occur on multiple length scales and vary depending on the location.[1-3] At the macroscopic level, surface roughness increases, especially near the exit plane where angled striations in the channel are formed. Near the anode deposition of metallic materials was evident. At the microscopic level, metallic atoms are deposited on the BN channel close to the anode and individual BN grains become smoother. Both Garnier, *et.al.*,[23-24] and Zidar, *et.al*.,[1-3] show that the chemical composition of the BN channel surface changes, with the fraction of silicon dioxide binding agent decreasing with proximity to the exit plane of the thruster. It is currently unclear how these surface changes affect SEE and sputter yield, and indirectly affect performance and lifetime.

The goal of this study is to develop methods for replicating the worn surface features of the BN channel without operating it for extended duration inside an HET. Future studies can then analyze the effects of changes in surface features on SEE and sputter yield without expensive long duration modification of samples by HET operation. In the following sections we present three manual modification methods to replicate the surface characteristics of a worn HET BN channel. Sandpaper and abrasive blaster modification methods were used for changing the surface roughness. Vacuum heating was used to attempt to modify the sample microstructure and chemical composition. Manually modified sample surfaces were characterized using surface profilometry, scanning electron microscopy, and electron dispersive spectroscopy. Manually modified surface characteristics are compared with those of worn HET samples to determine the modification methods that best replicate the worn HET channel surface.

II. Sample Surface Characterization Methods

Three surface characterization methods were used on the manually modified BN samples. Each sample was characterized using surface profilometry, scanning electron microscopy (SEM), and energy dispersive x-ray spectroscopy (EDS). Profilometry quantifies the surface roughness of the sample, while SEM provides a qualitative comparison of the microscopic topography of the samples. Energy dispersive x-ray spectroscopy (EDS) is used to quantify the atomic constituents on the surface of each sample.

A. Surface Profilometry

Surface profilometry determines surface roughness by measuring the height of finely spaced irregularities. Quantitatively, surface roughness is measured as the height of surface irregularities with respect to an average line. Roughness is expressed in units of length; in the case of this study, roughness is expressed in angstroms. In this investigation, roughness, termed R_a, is determined using the arithmetical average, as defined in Eqn. 1:

$$R_a = \frac{\sum_{i=1}^{n} y_i}{n} \tag{1}$$

For this investigation, surface profilometry is performed using a Sloan Dektak IIA surface measuring system. The Dektak IIA is capable of measuring surface features having heights ranging from less than 100 Å to 655,000 Å.[28] Calibration and verification of accurate roughness measurements are conducted both before and after the roughness studies performed using this instrument. In all cases the profilometer is found to be accurate within the specified ±5% for all standards measured, which covered the specified measurement range from 100 Å to 655,000 Å[28]. Scanning electron microscope images of the tracks made by the scanning stylus of the profilometer demonstrate that the profilometer stylus tip has a characteristic width of 10-15 μm. The geometry of the stylus tip is assumed to

be approximately hemispherical. The characteristic width of the stylus tip constrains the size of the surface features which can be measured in the direction of travel of the stylus tip. Therefore the profilometer can make vertical measurements of surface having characteristic heights in the range of 100's of Å, while the measurements of the horizontal lengths of these features are limited to the 10's of μm. This model profilometer is a single line profilometer, meaning the roughness can only be measured along a single line on the sample surface. To better ensure that the roughness measurements reflect the roughness of an entire sample surface, multiple scans were taken at multiple locations.

B. Scanning Electron Microscopy

A scanning electron microscope (SEM) uses electrons to produce images of surface features as low as 10 nm in size. An SEM operates by using an electron column consisting of an electron gun and two or more electrostatic lenses in a vacuum. The electron gun provides a beam of electrons having energies in the range of 1-40 keV, and the beam is reduced in diameter by electrostatic lenses to generate sharper images at high magnification. The electron beam interacts with the sample and penetrates roughly a micrometer into the surface, where electrons from the beam are backscattered and secondary electrons are emitted. Detectors collect the backscattered and secondary electrons, and these electron signals are used to generate the magnified image of the specimen.[31]

Secondary electrons emitted by the sample material are necessary to image the sample. Non-conducting insulators generally have poor secondary electron emission characteristics, in which case a conductive coating is often applied to provide high resolution, high magnification images. The ceramic specimens considered in this study are insulators, and a conductive coating is applied to provide the best imaging possible. In this study, a thin layer of 60:40 gold-palladium alloy is applied to the samples. The samples are placed into a vacuum chamber where the gold-palladium is sputtered onto the sample surface in a thin coat approximately 10 nm thick. The gold-palladium alloy provides high secondary electron emission, while still providing a thin, continuous film with minimal agglomeration regions. This thin coating provides the necessary secondary electrons for high resolution images, without obscuring the images of the underlying microstructure.

A Hitachi S-4700 scanning electron microscope was used to image the surface of each sample. It is capable of producing images with magnification greater than 500,000 times, and can resolve structures up to 2 nm across. For this investigation, micrographs were taken of each sample at magnifications of 30, 100, 400, 1,000, 5,000, and 10,000 times.

C. Electron Dispersive X-ray Spectroscopy

The SEM used in this investigation has energy dispersive x-ray spectroscopy (EDS) capability. EDS is a variant of x-ray fluorescence spectroscopy, and is used for chemical characterization and elemental analysis. EDS is performed by a SEM which has been installed with the necessary detection equipment. The electron column creates an electron beam focused on the sample surface. This focused electron beam results in the generation of an x-ray signal from the sample surface. The x-ray photons generated from the interaction of the focused electron beam and the sample surface pass through a beryllium window separating the specimen vacuum chamber and the Lithium-drifted Silicon detector. Within the detector, the photons pass into a cooled, reverse-bias *p-i-n* (p-type, intrinsic, n-type) Si(Li) crystal. The Si(Li) crystal absorbs each x-ray photon, and in response ejects a photoelectron. The photoelectron gives up most of its energy to produce electron-hole pairs, which are swept away by the bias applied to the crystal, to form a charge pulse. The charge pulse is then converted into a voltage pulse, which is then amplified and shaped by a series of amplifiers, converters, and an analog-to-digital converter where the final digital signal is fed into a computer X-ray analyzer (CXA).[31] A histogram of the emission spectrum from the sample is obtained and analyzed by the CXA to determine the percent by weight of elements present in the sample. For this study, EDS analysis was conducted using an EDAX energy dispersive x-ray unit attached to the Hitachi S4700 SEM. Data provided by EDS was the chemical composition of the sample regions by both percent of atoms and percent by weight.

III. Results

Samples of BN were manually modified. Two grades of BN were used. Grade HP is made of boron nitride and a calcium borate - boric acid binder mixture with a small amount of silica. Grade M26 is composed of a 60-40 mix by weight of boron nitride and silicon dioxide. These BN grades were modified using sandpaper manual abrasion, abrasive blasting, and vacuum heating. Results from surface characterization of manually modified samples are presented below. Surface roughness, surface images, and surface atomic composition results are presented from the

surface profilometry, SEM, and EDS analysis of sandpaper, abrasive blasting, and vacuum heating modified samples.

A. Sandpaper Manual Abrasion

Two samples of HP grade and two samples of M26 grade BN were modified with 120 grit sandpaper. Only one sample of each grade was modified with 60, 220, and 400 grit sandpaper. A sample of BN was secured to the bottom of a plastic pull tab, on top of which a 200 gram weight was placed to maintain a constant frictional force between the sample and sandpaper. The weight on the sample was held constant between different tests, and the distance the sample was dragged is done in measured increments. In between distance increments the orientation of the sample is rotated by 90 degrees in an attempt to give a more even wear pattern.

1. Surface Roughness

Each sample had 6 profilometer scans performed on it after each drag increment. As such each data point is the average of a set of 6 roughness values. The error bars in Figure 2 represent the standard deviation of each set of 6 roughness values.

Surface roughness measurements are presented in Figure 2 for samples modified with 120 grit sandpaper. Pristine surface roughness (distance of 0 cm) for M26 is 18500±6500 Å, while HP is 9600±760 Å. These measurements agree closely with those by Zidar.[1-3] Figure 2 shows that as the distance the weight is dragged across the sample increases, surface roughness increases. While grade HP is initially smoother than M26, after 3 cm, HP is 26% rougher than M26.

The grade M26 samples had an increase in roughness from the baseline of 60% and 25% respectively, while the HP samples had a roughness increase of 8 and 8.75 times respectively after the full 24 cm drag distance.

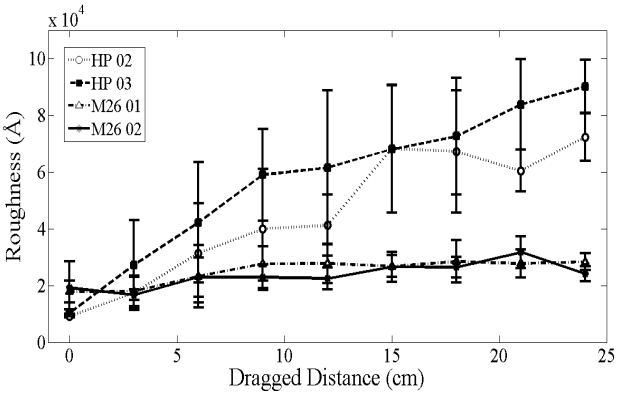

Figure 2. Surface roughness results for samples modified with 120 grit sandpaper.

2. SEM Images

Images of a sandpaper modified sample were taken after the final interval of abrasion was performed, that is after a drag distance of 24 cm. Due to the requirement of a conductive coating that has to be applied to the sample for imaging, samples are only imaged once they are finished with the specific experiment, to ensure that the coating agent does not affect the roughness measurements.

Figure 4 on the following page shows the SEM images of the sandpaper modified samples. At lower magnifications the groves from the sandpaper can be clearly seen. At higher magnifications (1000x) the grooves display an appearance more heterogeneous in color compared to the darker more uniform regions adjacent to them. The highest magnification images show plates made of many individual particles, arranged in a random orientation as a result of being disturbed by the abrasion process.

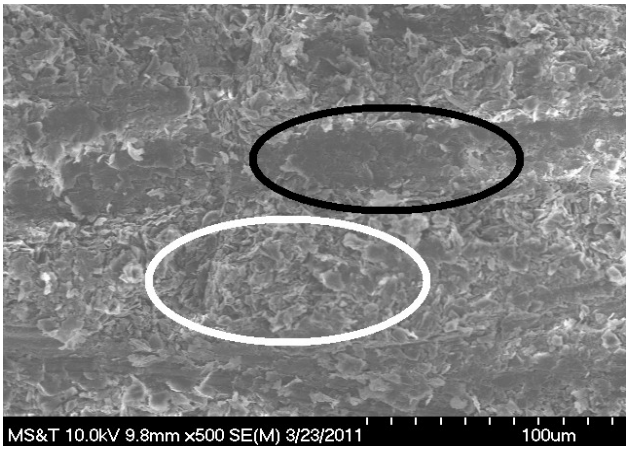

Figure 3. Example of homogeneous color regions compared to heterogeneous regions . *The white circle shows a region of jumbled color, the black circle show a undisturbed region of uniform color.*

Upon closer inspection in figure 3 the 10,000x magnification images the individual grains in the darker regions appear to have a more uniform orientation and undisturbed structure. This suggests that the more heterogeneous color regions are the regions that experienced damage from the sandpaper abrasion process.

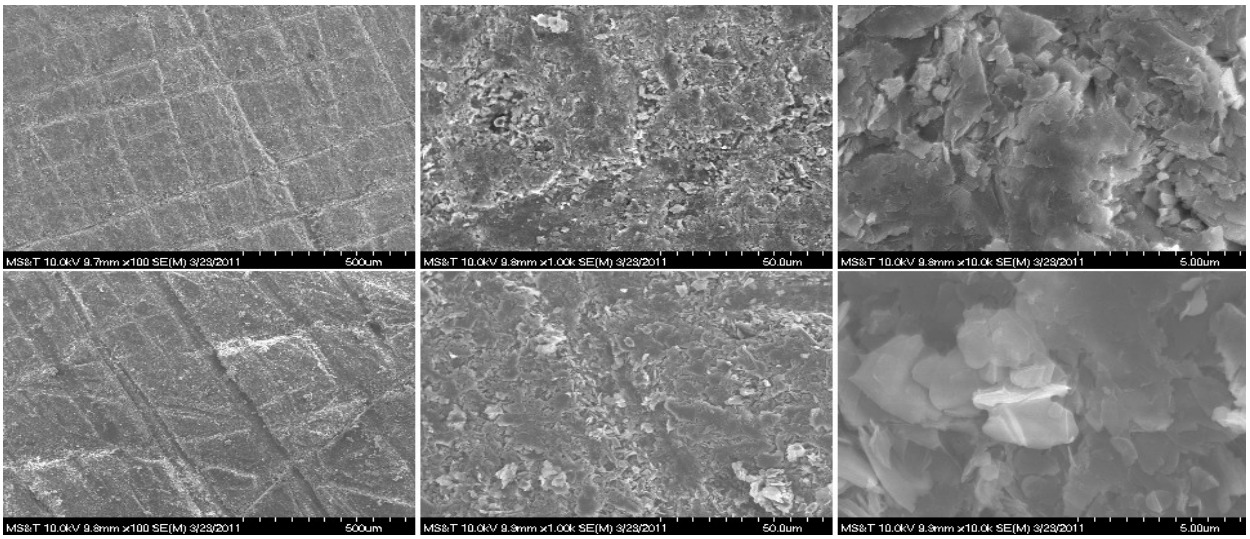

Figure 4. SEM images of 120 grit sandpaper test results. *The top row shows from left to right 100x, 1000x, and 10,000x magnification images of grade HP. The bottom row shows the same series of images for grade M26*

3. EDS Analysis

Analysis of the elemental composition of BN samples after modification with sandpaper show an increase in trace elements and oxygen content. Due to the imaging agent required to coat the sample for use in the SEM, all of the samples were unique and had only one test performed on them. For example the sample used for the pristine chemical analysis of grade HP was a different sample then the sandpaper abraded grade HP sample. Pristine grade HP is composed of 4.5% trace elements. Trace elements being those elements that are not boron, nitrogen, or oxygen. After modification the trace elements make up 10.9% of the weight of the grade HP sample. The pristine element composition of grade M26 is made up of 3.4% trace elements. After modification the trace elements account for 3.5% of the weight. Trace elements in grade M26 are those elements not boron, nitrogen, silicon, or oxygen. Of the non-trace elements oxygen has a 11.5% increase by weight in the grade HP sample, and a 12.5% increase by weight in the grade M26. Boron and nitrogen have a loss in weight of 5.5% and 11.4% in grade HP respectively, and 11.3% and 14.6% respectively in grade M26. Silicon has a 2% increase in grade M26. In grade HP silicon is considered a trace element and not used as a primary binding agent.

Table 1. Sandpaper EDS results

Grade HP	by weight	by weight	Grade M26	by weight	by weight
Element	Pristine	Sandpaper	Element	Pristine	Sandpaper
B	27.73	22.06	B	23.2	20.57
N	59.55	48.17	N	29.54	25.22
O	7.28	18.84	O	24.42	30.68
Si	0.19	0.5	Si	19.45	20.02
C	2.92	5.26	C	3.28	3.28
Ca	0.48	2.94	Na	0	0.12
Na	0	0	Al	0.12	0.11
F	0.95	1.83	K	0	0
Al	0	0.08	Ca	0	0
Cl	0	0.14	Cl	0	0
K	0	0.18	S	0	0

B. Abrasive Blaster

A sample of each grade of BN was modified with an abrasive blaster. A small tower was constructed to hold the model 260 Badger mini sandblaster at a constant height above the BN samples. The tower allows for an adjustable height to ensure that the cone of grit exiting the nozzle of the blaster can completely cover the sample. A height of 18 cm gave good sample coverage without eroding the sample too quickly. The samples of BN are exposed to the

abrasive grit in short increments of 2 seconds. The compressed air was supplied at 23 psi. The samples were abraded for an increment of time, then the roughness was investigated on the profilometer before another increment of abrasion.

1. Surface Roughness

Figure 5 shows the results of the abrasive blaster modification. Like the sandpaper samples, each data point is the average of 6 profilometer scans. The error bars represent the standard deviation of the 6 different scans. The grade HP sample has a roughness change of a factor of 5 over the course of the modification, while the M26 only has a 30% roughness increase. These trends agree with the sandpaper modification, and suggest that a difference in the composition between the two grades allows for M26 to be more resistant to abrasion. The samples under the abrasive blaster show a trend of leveling off at a maximum roughness value. This is especially clear in the HP sample which has a roughness increase by a factor of 4.3 after the first 5 seconds, but only a 25% increase from 5 seconds to 13 seconds.

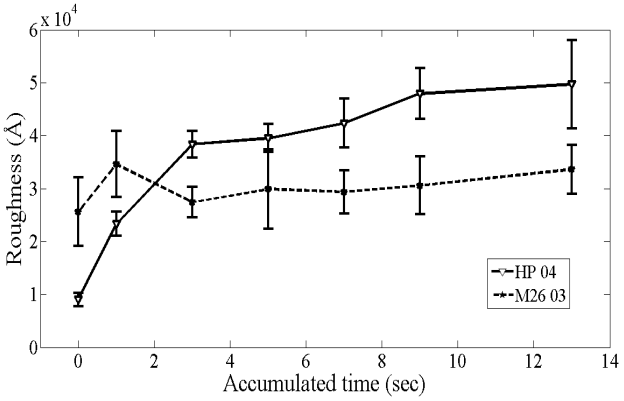

Figure 5. Abrasive blaster roughness results for 220 grit.

2. SEM Images

Abrasive blasted samples were also imaged, the images are shown in Figure 6. One of the interesting features on the lower magnification images, are the series of straight and perpendicular lines seen on the sample surfaces. The surface of the blasted samples can be described as powdery, this powder allows the needle on the profilometer to leave a trail in the loose material on the surface of the sample. This powdery material appears to be a deposition of grains and abrasive materials disturbed by the abrasive blasting process.

The higher magnification images show a grain structure similar to the sandpaper samples, and the shielded sections of actual thruster channels. But the powdery nature of the abrasive blaster samples results in what appears to be a more disrupted structure to the arrangement of the grains then seen in the other images. To the naked eye the layer of powdery material could not be seen, future abrasive blaster test will have the sample cleaned with compressed air.

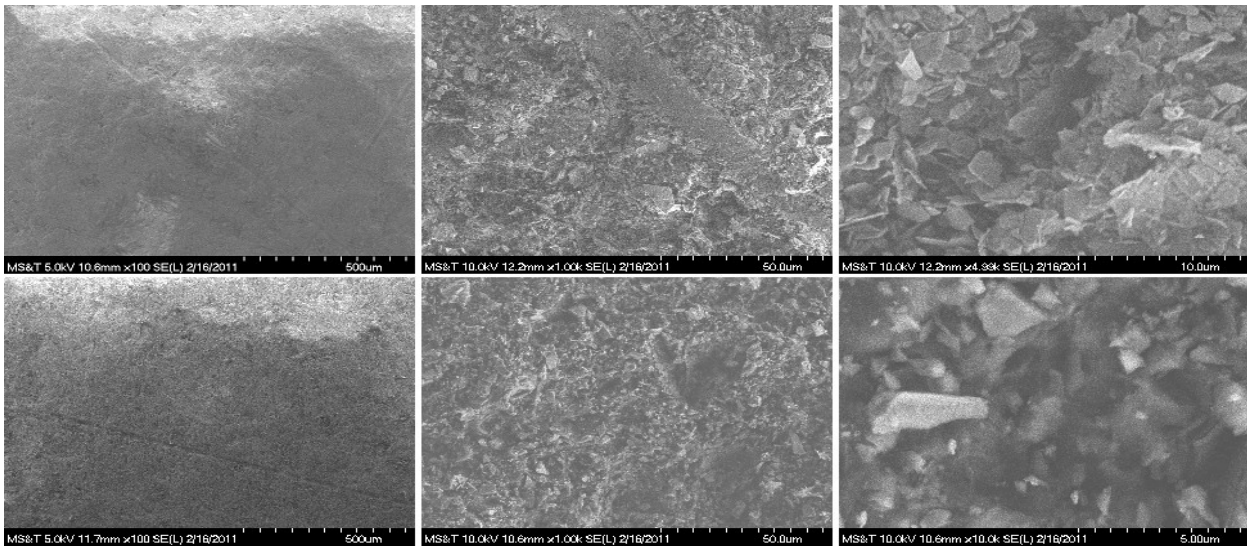

Figure 6. SEM images of abrasive blaster tests results. *The top row shows from left to right 100x, 1000x, and 10,000x magnification images of grade HP. The bottom row shows the same series of images for grade M26*

3. EDS Analysis

After modification of BN samples with the abrasive blaster an increase in trace elements and oxygen is observed. Grade HP is initially composed of 4.5% weight of trace elements, after modification the trace element weight percentage is 10.8%. The grade M26 sees an increase in trace element weight from 3.4% to 8.9%. The weight of oxygen in the samples increases after modification by 11.5% in grade HP and by 20.4% in grade M26. Boron and nitrogen have a loss of 5.3% and 11.5% respectively in grade HP, and a loss of 23.5% and 17.2% respectively in grade M26. Silicon remains constant in grade M26.

Table 2. Abrasive Blaster EDS results

Grade HP	by weight	by weight	Grade M26	by weight	by weight
Element	Pristine	Abrasive	Element	Pristine	Abrasive
B	27.73	22.45	B	23.2	17.74
N	59.55	48.02	N	29.54	24.43
O	7.28	18.72	O	24.42	29.42
Si	0.19	0.28	Si	19.45	19.46
C	2.92	4.96	C	3.28	6.54
Ca	0.48	3.07	Na	0	0.58
Na	0	0	Al	0.12	0.46
F	0.95	1.83	K	0	0.44
Al	0	0.33	Ca	0.01	0.19
Cl	0	0.14	Cl	0	0.59
K	0	0.18	S	0	0.15

C. Vacuum Heating

The anode at the base of the thruster channel can heat the channel wall to 400 C based on the work by Tomaszewski, et al.[27] The binder agent within the ceramic composition of the BN material has a significantly lower melting point than the boron nitride. Boric acid in the grade HP and silicon dioxide in the grade M26 melt at 550 C and 1700 C, respectively. Changes in material composition at various locations in the thruster have been observed by Zidar and Rovey.[1-3] These changes may be partially related to heat, or if not, it may be possible to replicate the changes through the use of heat treatments. Samples are heated in a Thermal Technology model 1100-4080-W3 furnace under high vacuum conditions. Temperatures of 400, 1000, and 1800 C are used to modify BN samples. The 400 C temperature replicates the temperature conditions of a running thruster.[27] The 1000 and 1800 C temperatures are chosen to study any effects that might result form the loss of the binding agent in the ceramic. The samples are each heated for 30 minutes.

1. Surface Roughness

Heat treated samples did not show a change in surface roughness. Any surface changes that happen to the sample due to heating are on a scale smaller than can be measured by the profilometer. The surface roughness of the unmodified sample of M26 was 27,218 Å, and after heating the roughness was 26,704 Å, well within the standard deviation of 3,117 Å seen on the pristine sample.

2. SEM Images

Images at the 10,000x magnification seen in Figure 7, most clearly show changes in the microstructure. The HP sample heated to 1800 C looks similar to the undisturbed sections of the other modified samples of grade HP. The individual grains on the HP sample do appear more rounded at the corners than the grains from the other methods of modification. The average grain size in grade HP shrinks with increasing temperature. In the 400 C image, the grains of BN are still connected to each other to form larger plates around 6 μm in size, where as in the 1800 C image, the grains of BN are separated from each other by more fracture lines, resulting in grains of 2 μm in size. The sample of M26 heated to 400 C shows a layered pattern of flat grains stacked horizontally on each other. This stacked patten is not prominently displayed in the 1000 C sample. The 1800 C sample of grade M26 was not able to be run with the other sample due to malfunctioning equipment.

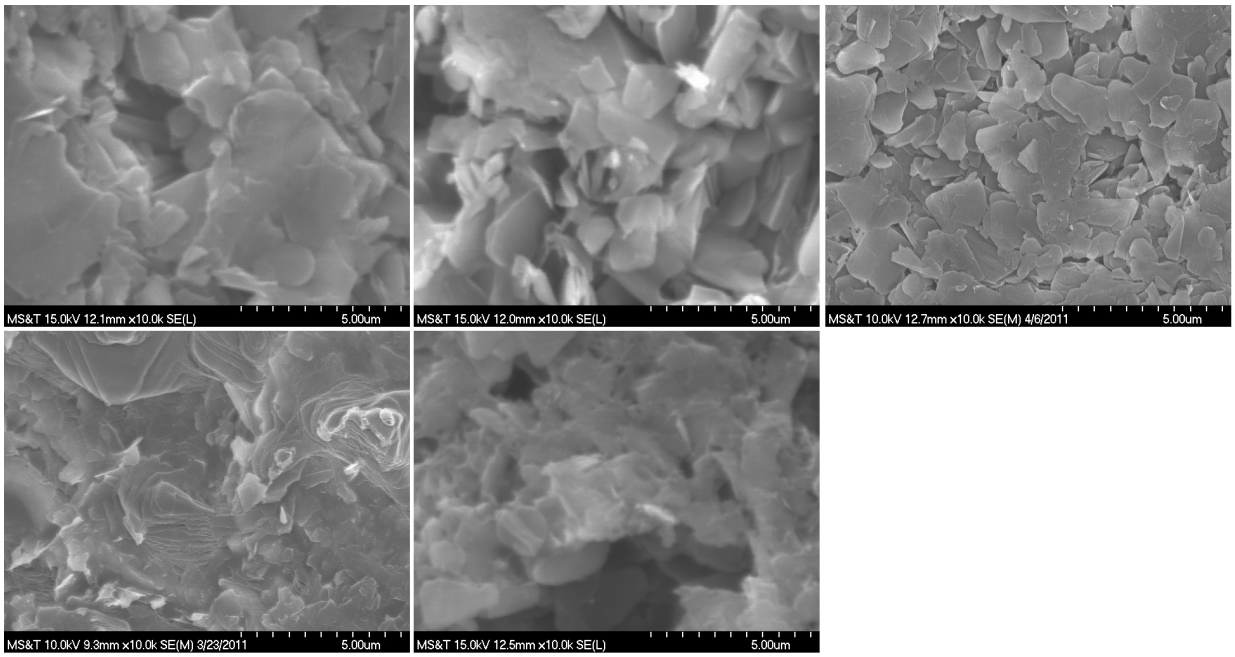

Figure 7. Heated sample microstructure. *The top row images are at 10,000x magnification of grade HP samples heated at 400, 1000, and 1800 degrees Celsius from left to right respectively. The Bottom row images are at 10,000x magnification of grade M26 samples heated at 400, 1000, and 1800 degrees Celsius from left to right respectively. The 1800C sample of grade M26 has not been completed.*

3. EDS Analysis

The EDS results seen in Table 3 show changes in the chemical composition of the samples. In the 1800 C sample boron and nitrogen are the only significant chemical signatures with boron decreasing by 8% and nitrogen increasing by 8% from the pristine sample weights, it is assumed that these elements represent the boron nitride compound. The 400 C sample of grade M26 has a 18% decrease in boron and a 13% decrease in nitrogen content from the pristine, and a corresponding 9% increase in silicon and a 19% increase in oxygen. The carbon is most likely a result of contamination from handling, as are the potassium and sodium. SEM and images and EDS analysis of the 1000 C sample of grade M26 show a significant source of contamination in the 21% value of calcium. This contamination stems from the equipment malfunction mentioned earlier. The SEM images of the contaminate structures suggests that they are a calcium based crystal. Not all of the samples have been heated and analyzed at the time of writing this, so further analysis will have to wait.

Table 3. Elemental composition by weight of heated samples.

Grade HP	by weight				
Element	Pristine	400 C	1000 C	1800 C	Listed
B	27.73	22.89	27.33	25.54	
N	59.55	47.55	63.71	64.57	
O	7.28	22.03	2.95	0.68	
Si	0.19	0.43	1.64	0	
C	2.92	1.94	3.88	4.12	
Ca	0.48	3.03	0.49	0	
Na	0	0.44	0	0	
F	0.95	0	0	0	
Grade M26	by weight				
Element	Pristine	400 C	1000 C	1800 C	Listed
B	23.2	19.57	11.79		26.5-28.7
N	29.54	25.31	25.52		32.8-35
O	24.42	29.85	28.3		21.33
Si	19.45	19.62	7.77		18.67
C	3.28	3.33	1.57		0
Na	0	1.17	0		0
Al	0.12	0.15	0		0
K	0	0.98	0		0
Ca	0	0	21.55		0.01

IV. Discussion

Using the results previously discussed, the following sections discuss the manual modification methods ability to reproduce wear characteristics of worn HET discharge channels. The results of the sandpaper and abrasive blaster experiments are discussed with respect to how roughness values are influenced by material properties. Of the completed vacuum heating results, some of the interesting features are commented on as well.

A. Roughness by Manual Abrasion

The change in roughness is a function of the sample grade, abrasive material, and time or distance abraded. At the beginning of the abrasion process the time or distance is the most important variable in determining the roughness. However after a short number of iterations of abrasion the time or distance becomes less important to the roughness value compared to the effect of the grit used to modify the sample.

1. Time or Distance Independent Roughness

There appears to be a limiting trend to the maximum roughness a sample can achieve from a given grit abrasive, shown in Figure 8. To study this maximum roughness, samples are abraded for roughly two times the maximum distance or time used in the incremented tests, this means 20 seconds in the blaster, or 40 centimeters on the sandpaper. This excessive

Table 4: Comparison of modification methods to properties changed.

	Roughness	Microstructure	Chemical Composition
Sandpaper	✓	x	x
Abrasive blaster	✓	x	x
Vacuum Heating	x	✓	✓

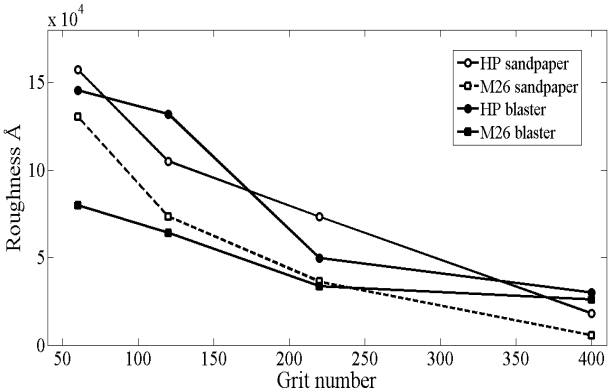

Figure 8. Effect of grit number on maximum roughness results.

duration of abrasion ensures that the maximum roughness value will have been met as seen by the decreasing slope between later data points in figures 2 and 5.

The graph in figure 8 shows a decreasing roughness with increasing grit number, as would be expected with smaller particles carrying less energy and therefore causing less damage to the sample surface. Similar to the incremented sandpaper and abrasive blaster tests, the M26 has a lower roughness for every grit number compared to the grade HP. The sandpaper modifications show a more uniform trend of roughness to grit than the abrasive blaster The scale of the abrasion damage and therefore the corresponding roughness value is a function of impact particle size, speed, and angle of incidence, as well as impacter material properties and surface material properties with the specific relation of these variables still under investigation. The abrasive blaster has a higher roughness at the higher grit values than the sandpaper. The higher roughness and more non uniform trend, of the abrasive blaster test stems from how the grit application method affects existing features on the sample surface. Tooling marks and macroscopic surface features cause higher roughness values to be seen by the profilometer. The abrasive blaster applies grit evenly across the entire surface area of the sample equally roughing the peaks and valley of existing surface features like tool markings, while the sandpaper abrasion gives emphasis to eroding the peaks of structures first resulting in a more level surface after modification as the peaks of preexisting tooling marks are worn down.

2. Importance of Grit

Apart from time or distance abraded at low numbers of iterations of drags or blasts, the grit size of the abrasive has the strongest effect on the roughness of the samples. Lower number grits result in higher roughness values. At the 60 grit abrasion the samples became more difficult to measure due to the size of the features becoming close to the maximum difference the profilometer was capable of measuring.

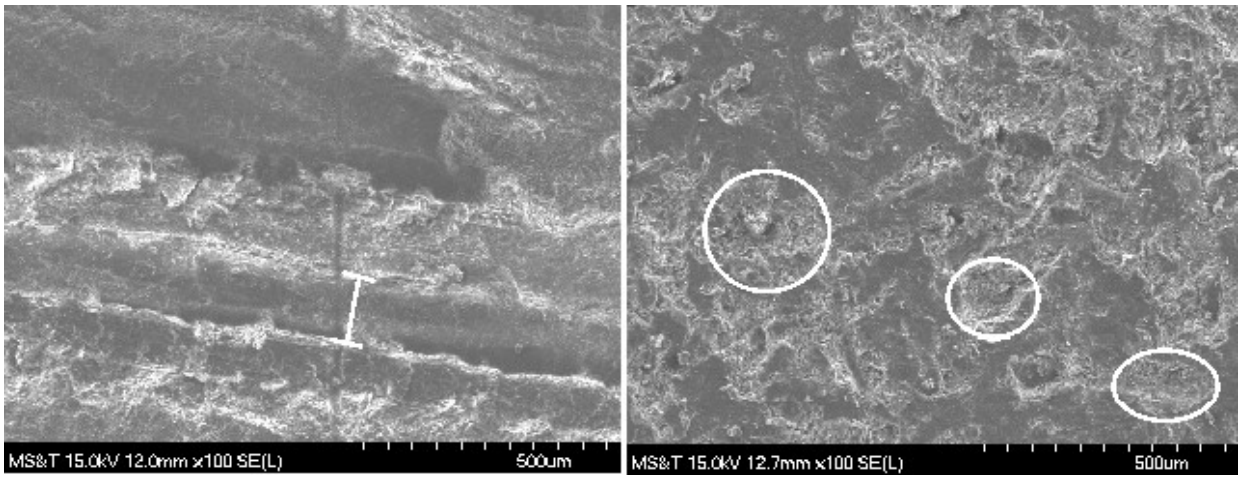

Figure 9. Pits created by particle bombardment from 60 grit abrasive blaster. *The white line in the left image shows the peak to peak distance of a groove crave out by sandpaper abrasion. The groove has a width of 150 μm and runs the length of the sample surface. The white circles in the right image highlight pits caused by particle impact. The distinguishable carters have a size range of 250 μm to 200 μm Both images are at 100x magnification.*

The method of application of the grit also shows some effect on the maximum roughness. The abrasive blaster on average gives the samples a lower roughness than sandpaper of the same grit at grit values above 220. This result is from the difference in how the grit modifies the surface, and the force with which the grit is applied to the sample surface. The sandpaper leaves long straight grooves in the surface as shown in the left image of figure 9. the groove runs the length of the sample surface and is roughly 150 μm wide. The abrasive blaster leaves small pits where the grit particles impact the surface of the samples. The pits highlighted in figure 9 appear to be the result of a single particle impact of slightly over 200 μm in diameter, which is comparable to the 265 μm average particle size of a 60 grit particle. This allows a single particle of grit to affect a significantly larger area of the sample under the sandpaper method as compared to the abrasive blaster method. Affecting a larger area of the sample gives the feature a much better chance of being detected by a profilometer pass.

3. Importance of Ceramic Grade

Throughout all of the abrasive tests the grade M26 has a lower roughness for the same grit value than the grade HP. The difference in the roughness suggests that the difference in chemical composition of the grades has an effect

on how the samples erode. The grade HP has boric acid as a binding agent, where as M26 uses silicon dioxide as a binding agent. The use of different binding agents has to account for the differences seen in the erosion of the two grades as all the other variables in the abrasion tests were held constant.

B. SEM Results Discussion

The SEM images show that although the numeric values of roughness could match the actual thruster channels, the microstructures could not be replicated. Specifically the knobby microstructures seen in 10,000x images of the actual thruster channels figure 10, were not seen. The microsturctures that were seen in the abraded samples did match well with the pristine and shielded sections of the actual thruster channels.

The heated samples showed variations in their microstructures compared to the abraded samples. The microstructures in the 400 C sample figure 7 show a more organized structure than is seen in the other samples. The grains appear to be stacked flat on top of each other. The 1800 C sample showed more rounding on the corners of the grains, but the grains still appeared to be flat rather then the spherical knobs seen in the actual thruster channels and shown in figure 10. However the 10,000x image of the pristine HET in figure 11 has grains that look very similar to the grains in the 400C sample of grade HP.

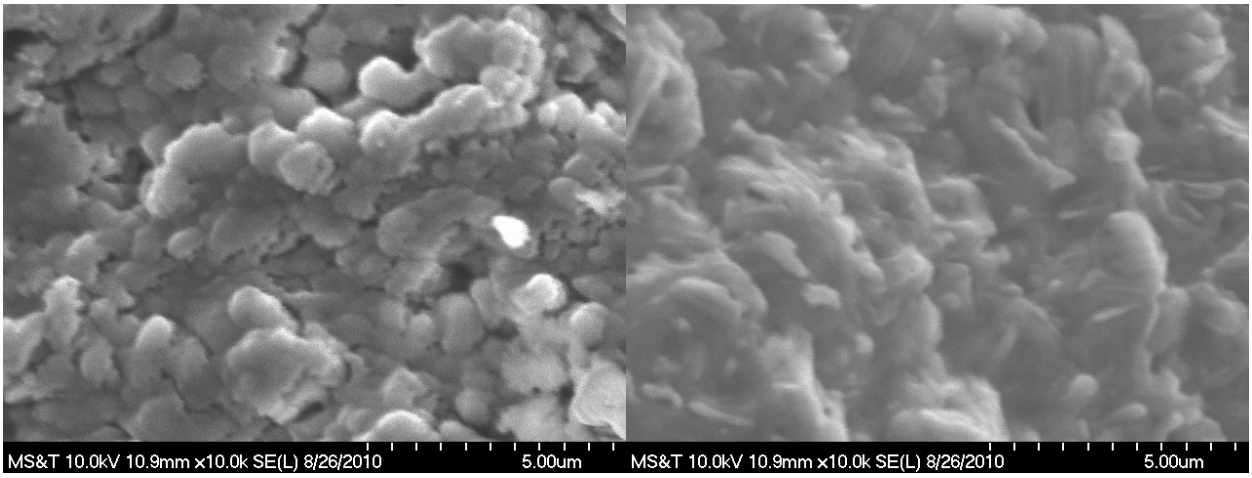

Figure 10. Knobby microstructures. *Both images are taken at 10,000x magnification and are of worn HET discharge channels. The image on the left is from the anode region, the image on the right is from the exit plane.*

The anode region of the thruster channel experiences less high energy bombardment and experiences more heat as a result of the proximity to the heated anode the similarity between the vacuum heated samples, figure 7, and the worn HET shielded sections, figure 11, suggest that in the localized region heat may play a larger factor in determining wear characteristics than ion bombardment. At the time of writing this, not all of the heated samples have been analyzed, so further discussion will wait for more results.

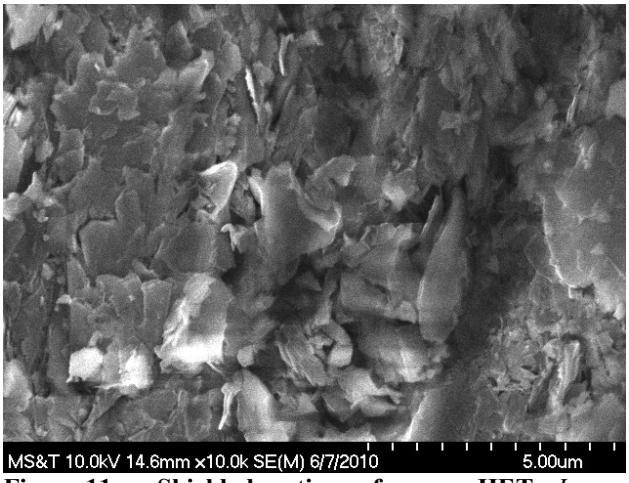

Figure 11. Shielded sections of a worn HET. *Image taken at 10,000x magnification*

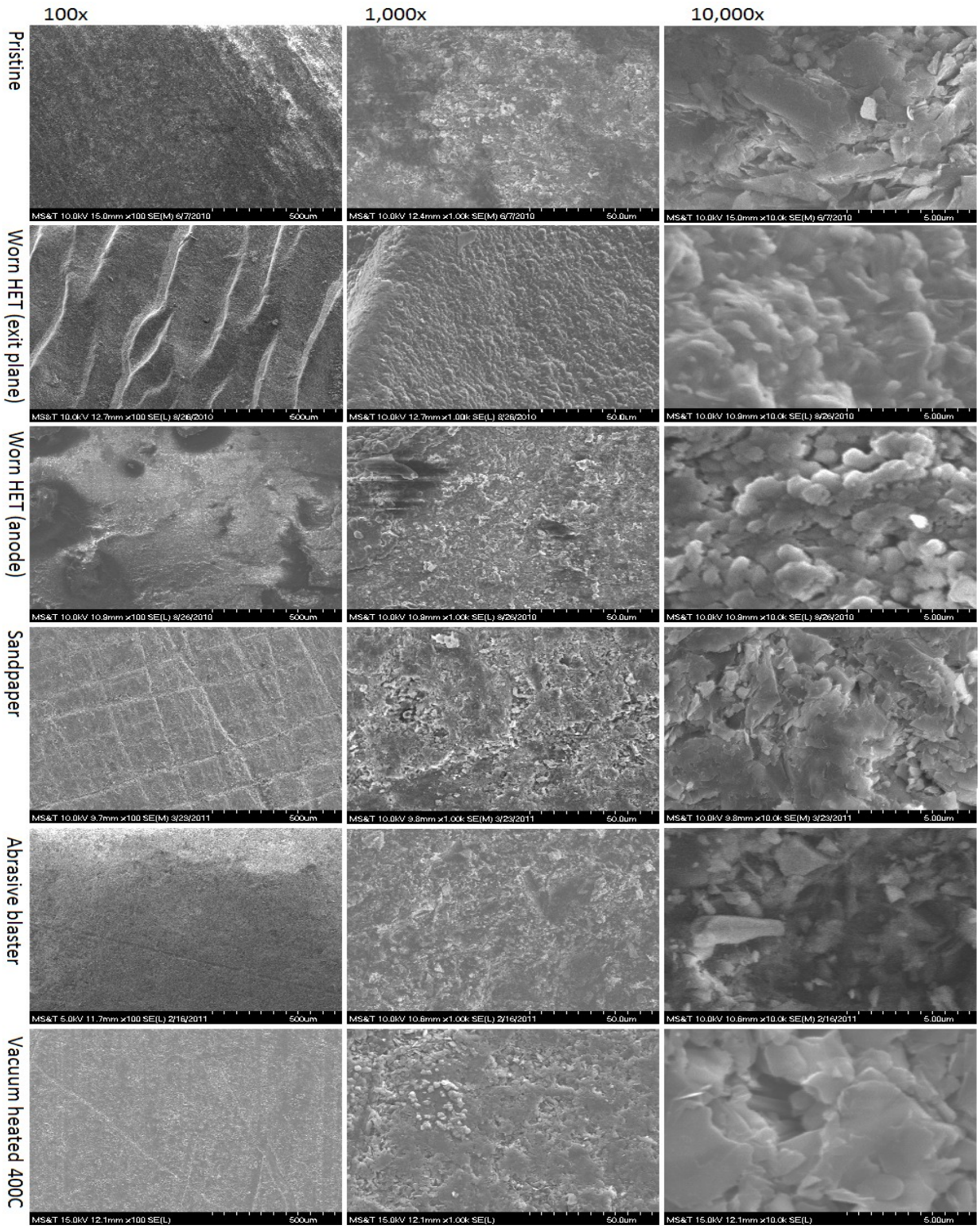

Figure 12. Comparison of all modification methods under SEM inspection. *Images at 100x, 1000x and 10,000x magnification are shown ordered by modification method. Each modification method has only one samples images shown as a typical example of features seen under SEM inspection for that particular modification method. Pristine, exit plane, sandpaper, and abrasive blaster are of grade M26.Anode, and vacuum heated are of grade HP.*

C. EDS Results Discussion

1. Abrasion sample EDS

As expected of the abrasive modified samples, after modification trace elements not present in the listed or pristine results appeared. Aluminum is a result of the aluminum oxide grit used in both the abrasive blaster and on the sandpaper. Potassium, sodium, calcium, carbon and chlorine are most likely deposited when handling the samples in between abrasion and imaging.

Of particular interest was the nearly 10% increase in oxygen seen across all grades and abrasion methods as compared to the pristine samples. The amount of extra oxygen is great enough based on stoichiometric analysis that another source besides left over abrasive aluminum oxide must be contributing oxygen to the sample. For example in the grade M26 sandpaper abraded sample table 1 has a 7.8% total weight of oxygen not bound in the formation of silicon dioxide. Assuming all of the trace aluminum is used the the formation of aluminum oxide, the oxygen used only accounts for 3.1% of the extra oxygen weight. Another source of oxygen is a thin film of B2O3 that can form on the sample surface in the presence of air, as reported by Leichtfried *et al*.,[30] . Using the same grade M26 sample mentioned above, assuming a maximum yield of boron nitride based on the EDS elemental weights once all of the nitrogen is used, there is still 1% of the sample weight that is composed of boron not used in the formation of boron nitride. This extra boron is likely to be the boron involved in the creation of B2O3, which accounts for a further 2.4% of the extra oxygen weight. A further possible cause of the extra oxygen may be due to the hygroscopic nature of boron nitride. The last 2.3% of oxygen weight not accounted for by AL2O3 and B2O3 could be from water trapped in the sample, keeping in mid that hydrogen can not be seen through EDS analysis. With the manual abrasion methods significantly increasing the surface area of the sample, a film of B2O3 could account for a 30% of the increase in oxygen seen on the EDS results along with contributions from other residual oxides, trapped water and from handling and abrasive compound residues accounting for the rest of the increase.

2. Heated sample EDS

The grade HP sample showed a loss of many of the binding agent elements beginning at the 1000 C sample. The melting point of boric acid, the primary binding agent in grade HP, is 550 C. Between the 400 C sample and the 1000 C sample the oxygen content goes from 22% to 3%. The 1800 C sample further supports this conclusion with an oxygen amount of less than 1%. It is likely that the oxygen present in the 1800 C sample is not from the original oxygen containing compounds in the sample, but is from B2O3 contamination from the air after heating, as was seen on the EDS of the abraded samples.

In comparison to the HP sample, the M26 sample shows a slight increase in SiO2, with a corresponding decrease in boron nitride. These results are unexpected under the assumption that SiO2 is the first part of the ceramic to be lost under heating conditions given the melting temperature of boron nitride is 2900 C compared to the 1700 C melting point of SiO2.

It should be noted that for each temperature level, a different sample had to be used. This is a result of having to coat the samples in gold-palladium for use in the SEM. While care was taken to ensure that all of the samples came from the same block of material, inhomogeneities within the block could affect the local distribution of elements in the sample.

V. Conclusion

Sandpaper and abrasive blaster modification methods have both shown the ability to match the numerical roughness values seen at any location in a worn HET as measured by Zidar, *et.al*.,[1-3] However the structures responsible for roughness values in worn HET's look substantially different from the structures created by both methods of abrasion. The recommended method to match a pristine samples surface roughness value to a worn samples roughness value would be to choose a grit size based on the data in figure 8 that produces a maximum roughness after prolonged abrasion which matches the worn roughness value.

Vacuum heating has shown an ability to modify the microstructures and chemical composition of the samples. So far there appears to be a resemblance between the shielded sections of the worn HET, and the heated samples microstructure. However other microstructures seen in the worn HET have yet to be reproduced. Heating can be used to modify the amount of binding agent in the BN samples, with a wider range of heated data points it may be possible to replicate specific ratios of boron nitride to binding agent seen at different locations in the worn HET.

References

[1] Zidar, D. G., "Hall-effect Thruster Surface Properties Investigation," Masters Thesis, Dept. of Aerospace Engineering, Missouri University of Science & Technology, Rolla, MO, 2011.

[2] Zidar, D. G., Rovey, J. L., "Boron Nitride Hall-effect Thruster Channel Surface Properties Investigation," AIAA-2011-5993, *47th Joint Propulsion Conference*, San Diego, CA, July 31 - Aug 3, 2011.

[3] Zidar, D. G., Rovey, J. L., "Hall-effect Thruster Channel Surface Properties Investigation," *Journal of Propulsion and Power*, accepted 9/2011.

[4] Fife, J. M., Gibbons, M. R., Hargus, W. A., VanGilder, D. B. and Kirtley, D. B., "3-D Computation of Surface Sputtering and Redeposition Due to Hall Thruster Plumes," *International Electric Propulsion Conference*, IEPC, 2003.

[5] Hofer, R. R., Mikellides, I. G., Katz, I. and Goebel, D. M., "Wall Sheath and Electron Mobility Modeling in Hybrid-PIC Hall Thruster Simulations," *43rd AIAA/ASME/SAE/ASEE Joint Propulsion Conference and Exhibit*, AIAA, 2007.

[6] Ivanov, A. A., Ivanov Jr., A. A. and Bacal, M., "Effect of plasma-wall recombination on the conductivity of Hall thrusters," *Plasma Physics and Controlled Fusion*, Vol. 44, No. 7, 2002, pp. 1463-1470.

[7] Sommier, E., Allis, M. K., Gascon, N. and Cappelli, M. A., "Wall Erosion in 2D Hall Thruster Simulations," *42nd AIAA/ASME/SAE/ASEE Joint Propulsion Conference and Exhibit*, AIAA, 2006.

[8] Sullivan, K., Fox, J., Martinez-Sanchez, M. and Batischev, O., "Kinetic Study of Wall Effect in SPT Hall Thrusters," *40th AIAA/ASME/SAE/ASEE Joint Propulsion Conference and Exhibit*, AIAA, 2004.

[9] Locke, S., Shumlak, U. and Fife, J. M., "Effect of a Channel Wall Discontinuity in an SPT-Type Hall Thruster," *37th AIAA/ASME/SAE/ASEE Joint Propulsion Conference*, AIAA, 2001.

[10] Morozov, I A., "The Conceptual Development of Stationary Plasma Thrusters," *Plasma Physics Reports*, Vol. 29, No. 3, 2003, pp. 235-250. (Translated from Russian. Originally published in *Fizika Plazmy*, Vol 29, No, 3,pp. 261-276.)

[11] Raitses, Y., Staack, D., Keidar, M. and Fisch, N. J., "Electron-wall interaction in Hall thrusters," *Physics of Plasmas*, Vol. 12. No. 5, 2005, pp. 057104-1 – 057104-9.

[12]Dunaevsky, A., Raitses, Y. and Fisch, N. J., "Secondary electron emissions from dielectric materials of a Hall thruster with segmented electrodes," *Physics of Plasmas*, Vol. 10, No. 6, 2003, pp. 2574-2577.

[13] Raitses, Y., Smirnov, A., Staack, D. and Fisch, N. J., "Measurements of secondary electron emission effects in the Hall thruster discharge," *Physics of Plasmas*, Vol. 13, No. 1, 2006, pp. 014502-014502-4.

[14] Peterson, P. Y., Jacobson, D. T., Manzella, D. H. and John, J. W., "The Performance and Wear Characterization of a High-Power High-Isp NASA Hall Thruster," *41st AIAA /ASME/SAE/ASEE Joint Propulsion Conference and Exhibit*, AIAA, 2005.

[15] Mason, L. S., Jankovsky, R. S. and Manzella, D. H., "1000 Hours of Testing on a 10 Kilowatt Hall Effect Thruster," *37th AIAA /ASME/SAE/ASEE Joint Propulsion Conference and Exhibit*, AIAA, 2001.

[16] Gorschkov, O., Shagayda, A. and Muravlev, V., "The Experience of Hall Thruster Research and Development," *57th International Astronautical Congress*, IAC, 2006. pp. 1-8.

[17] de Grys, K., Mathers, A., Welander, B. and Khayms, V., "Demonstration of 10,400 Hours of Operation on a 4.5 kW Qualification Model Hall Thruster," *46th AIAA/ASME/SAE/ASEE Joint Propulsion Conference &Exhibit*, AIAA, 2010.

[18] Sydorenko, D., Smolyakov, A., Kaganovich, I. and Raitses, Y., " Kinetic Simulation of Effects of a Secondary Electron Emission on Electron Temperature in Hall Thrusters," *The 29th Annual International Electric Propulsion Conference*, IEPC, 2005.

[19] Zhurin, V. V., Kaufman, H. R. and Robinson, R. S., "Physics of closed drift thrusters," *Plasma Sources Science and Technology*, Vol. 8, No. 1, 1999, pp. R1-R20.

[20] Choueiri, E. Y., "Fundamental Difference Between the Two Hall Thruster Variants," *Physics of Plasmas*, Vol. 8, No. l, 2001, pp. 5025-5033.

[21] Gascon, N., Dudeck, M. and Barral, S., "Wall material effects in stationary plasma thrusters. I. Parametric studies of an SPT-100," *Physics of Plasmas*, Vol. 10, No. 10, 2003, pp. 4123-4136.

[22] Yong, Y. C., Thong, J. T. L. and Phang, J. C. H., "Determination of secondary electron yield from insulators due to a low-kV electron beam," *Journal of Applied Physics*, Vol. 84, No. 8, 1998, pp. 4543-4548.

[23] Garnier, Y., Viel, V., Roussel, J. F. and Bernard, J., " Low-energy xenon ion sputtering of ceramics investigated for stationary plasma thrusters," *Journal of Vacuum Science and Technology*, Vol. 17, No. 6, 1999, pp. 3246-3254.

[24] Garnier, Y., Viel, V., Roussel, J. F., Pagnon, D., Mange, L. and Touzeau, M., "Investigation of Xenon Ion Sputtering of One Ceramic Material Used in SPT Discharge Chamber," *26th International Electric Propulsion Conference*, IEPC, 1999, pp. 512-517.

[25] Tondu, Th., Viel-Inguimbert, V., Roussel, J. F. and D'Escrivan, S., "Hall Effect Thrusters ceramics sputtering yield determination by Monte Carlo simulations," *44th AIAA/ASME/SAE/ASEE Joint Propulsion and Exhibit* , AIAA, 2008.

[26] Peterson, P. Y. and Manzella, D. H., "Investigation of the Erosion Characteristics of a Laboratory Hall Thruster," *39th AIAA/ASME/SAE/ASEE Joint Propulsion Conference and Exhibit*, AIAA, 2003.

[27] Tomaszewski, James, et al., "Characterization of a Hall Effect Thruster Using Thermal Imaging," *45th AIAA Aerospace Sciences Meeting and Exhibit,* Reno, NV, 2007, AIAA 2007-0584

[28] Sloan Technology Corporation, *Dektak IIA Manual*, Sloan Technology Corporation, Santa Barbara, CA, 1984, p. i.

[29] —. Combat® Solid Boron Nitride Composite Grade HP. [Online] February 2006. [Cited: September 9, 2010.] http://www.bn.saint-gobain.com/uploadedFiles/SGbn/Documents/Solids/Solid-Combat-BN-GradeHP.pdf.

[30] —. Combat® Solid Boron Nitride Composite Grades M and M26. [Online] June 2003. [Cited: September 9, 2010.] http://www.bn.saint-gobain.com/uploadedFiles/SGbn/Documents/Solids/Solid-Combat-GradesM-M26.pdf.
[31] Goldstein, J. I., Newbury, D. E., Echlin, P., Joy, D. C., Romig, Jr., A. D., Lyman, C. E., Fiori, C. and Lifshin, E., *Scanning Electron Microscopy and X-ray Microanalysis. 2nd edition*, Plenum Press, New York. 1992. pp. 21-25,292-311.
[32] P. Beiss, G. Leichtfried et al. (2002). "13.5 Properties of diamond and cubic boron nitride". *Landolt-Börnstein– Group VIII Advanced Materials and Technologies: Powder Metallurgy Data. Refractory, Hard and Intermetallic Materials.* 2A2. Berlin: Springer. pp. 118– 139. doi:10.1007/b83029. ISBN 978-3-540-42961-6.